Detection of Grid Voltage Fundamental and Harmonic Components Using Kalman Filter Based on Dynamic Tracking Model

Xiaohua Nie, *Member, IEEE*

***Abstract*—The Kalman filter (KF) algorithms based on traditional models, which, applied in real-time detection of grid voltage, have the margin to improve tracking accuracy. Their tracking models do not specify the covariance matrix of state noise in theoretical derivation. They can only be taken as a unit matrix. In this paper, a dynamic tracking model (DTM) is proposed. Further, a linear KF algorithm based on DTM model (DTM-KF) is presented. The proposed DTM-KF algorithm gives the covariance matrix of state noise and overcomes the defects of the traditional models based KF algorithms. It is compared with two traditional models–based KF algorithms by simulation and experimentation. The tracking accuracy of the fundamental component and the estimation accuracy of the harmonic components are analyzed and compared. The results show that the proposed DTM-KF algorithm has high tracking accuracy.**

***Index Terms*—Detection of grid voltage, dynamic tracking model (DTM), fundamental waveform tracking, harmonic estimation, Kalman filter (KF), covariance matrix of state noise.**

I. Introduction

THE Kalman filter (KF), which is widely used in some industrial fields, represents its advantages such as zero steady-state error, high real-time performance, better division of signal state and noise, etc. [1]. It plays an increasingly important role in the real-time detection of power quality disturbances. For example, it applies to the following fields such as harmonic estimation and control [2]–[17], frequency estimation [18]–[25], phase-locked loop synchronization [20]–[25], phase estimation [26]–[31], voltage flicker estimation [32]–[35], power quality disturbance detection and classification [36]–[38], waveform envelope detection of ac signals for power quality control equipment [39]–[44], voltage sags detection for dynamic voltage restorers [45]–[48] and islanding detection in new energy generation system [49], [50], and so on.

Manuscript received July 25, 2018; revised November 6, 2018 and December 19, 2018; accepted January 20, 2019. Date of publication February 15, 2019; date of current version September 30, 2019. This work was supported by the National Natural Science Foundation of China under Grant 51467013 and Grant 51867017.

The author is with the Department of Energy and Electrical Engineering, Nanchang University, Nanchang 330031, China (e-mail: niexiaoh@163.com).

Color versions of one or more of the figures in this paper are available online at http://ieeexplore.ieee.org.

Digital Object Identifier 10.1109/TIE.2019.2898626

Existing KF-based power quality disturbance real-time detection methods include linear and nonlinear methods. Either linear or nonlinear KF method needs to be based on an accurate model description for distorted ac signal. However, the nonlinear KF methods use several approximate linearization tracking models, such as Taylor expansion approximation, probability density approximation, and so on [4], [6], [9], [20], [38]. The existing linear KF methods based on traditional tracking models yet have limitation to improve tracking accuracy that their covariance matrices of state noise cannot be clearly given. They can only be taken as a unit matrix [3], [21]–[24], resulting in a lack of correlation between the estimated vectors. However, the association is inevitable from the theoretical analysis of stochastic process [51].

This paper contributes to a new linear KF method based on dynamic tracking model (DTM) for real-time detection of grid voltage fundamental and harmonic components. This method theoretically gives the covariance matrices of state noise. So, it clearly correlates with the state noise between the estimated vectors.

The rest of this paper is organized as follows. In Section II, the related work is reviewed. In Section III, the DTM model is proposed in detail. The state space of the DTM is extended. A new KF algorithm based on the proposed DTM model (DTM-KF) is presented. In Section IV, the performances of DTM-KF algorithm are evaluated and compared with the two traditional algorithms by simulation. In Section V, the effectiveness of DTM-KF algorithm is analyzed and compared through the experimental sampling data. Section VI concludes this paper.

II. Related Work

In this section, the existing KF methods are reviewed briefly. Two traditional models of the phase angle vector (PAV) and the orthogonal vector (OV) model are introduced. The KF algorithms based on PAV and OV models are widely used in the phase-locked loop synchronization, power quality disturbance detection, harmonic estimation, etc. [2], [3], [21]–[25].

A. Brief Review on Existing KF Method

Dr. A. A. Girgis took the lead in applying the KF to the power signal processing fields in 1981 [2], [3]. Existing KF-

TABLE I
KF-BASED POWER QUALITY DISTURBANCE DETECTION METHODS

Linear KF	Tracking models	PAV model, OV model.
	Algorithms	KF, H$^{\infty}$KF, STF, EnKF , etc.
Nonlinear KF	Tracking models	Approximate models.
	Algorithms	EKF,UKF, CKF , etc.

based power quality disturbance detection methods are shown in Table I.

So far, there are two kinds of tracking models for linear KF algorithm. The one is the PAV model–based KF algorithm (PAV-KF) [2], [3]. The other is the OV model–based KF algorithm (OV-KF) [3], [21], [22]. Moreover, the suboptimal linear and nonlinear KF algorithms are generally used to improve the estimation results. The suboptimal linear KF algorithms include H$^{\infty}$KF [19], [38], strong tracking KF (STF) [28], [45], and Ensemble KF (EnKF) [15]. The nonlinear KF algorithms include extended KF (EKF) [6], [20], unscented KF (UKF) [9], [38], and cubature KF (CKF) [4].

The KF-based power quality disturbance detection methods required the dimension expansion of the state space. Owing to the low-order harmonics components existing in the distorted ac signals [16], [17], [41], [46], the energy distribution between low-order harmonics and random signals has a huge difference. The waveform of the distorted ac signal sampled at time t can be expressed as

$$x(t) = \sum_{i=1}^{N} A_i(t)\sin[i\omega_0 T + \theta_i(t)] + \sum_{i=1}^{N} w_i(t) \tag{1}$$

where $i = 1, 2, 3, \ldots, N$ and T is the sampling cycle. For the fundamental frequency of 50 Hz, $\omega_0 = 100\pi$. $\sum_{i=1}^{N} A_i(t)\sin[i\omega_0 T + \theta_i(t)]$ is the fundamental and harmonic components. $\sum_{i=1}^{N} w_i(t)$ is the state noise of fundamental and harmonic components.

B. PAV Model

The PAV model uses the phase angle as a vector to establish a state space model through cosine expansion [2], [3]. The vector of fundamental and harmonic components is expressed as $X_k = [\,x_1\ x_2\ \cdots\ x_{2n-1}\ x_{2n}\,]^T$, where $x_1 = A_1\cos\theta_1$, $x_2 = A_1\sin\theta_1$, $x_{2n-1} = A_n\cos\theta_n$, and $x_{2n} = A_n\sin\theta_n$.

The measurement equation of PAV model is expressed as

$$z_k = H_k X_k + V_k = \begin{bmatrix} cos(\omega_0 kT) \\ -\sin(\omega_0 kT) \\ \vdots \\ \cos(\omega_0 kT \\ -\sin(\omega_0 kT) \end{bmatrix}^T \begin{bmatrix} x_1 \\ x_2 \\ \vdots \\ x_{2n-1} \\ x_{2n} \end{bmatrix}_k + V_k. \tag{2}$$

The state equation of PAV model is expressed as

$$X_{k+1} = \Phi_k X_k + W_{\mathrm{k}} = \begin{bmatrix} x_1 \\ x_2 \\ \vdots \\ x_{2n-1} \\ x_{2n} \end{bmatrix}_{k\,k+1}$$

$$= \begin{bmatrix} 1 & 0 & \cdots & 0 & 0 \\ 0 & 1 & \cdots & 0 & 0 \\ \vdots & \vdots & \vdots & \vdots & \vdots \\ 0 & 0 & \cdots & 1 & 0 \\ 0 & 0 & \cdots & 0 & 1 \end{bmatrix} \begin{bmatrix} x_1 \\ x_2 \\ \vdots \\ x_{2n-1} \\ x_{2n} \end{bmatrix}_k + \begin{bmatrix} W_1 \\ W_2 \\ \vdots \\ W_{2n-1} \\ W_{2n} \end{bmatrix}_k. \tag{3}$$

The covariance matrix of state noise W_k for PAV model can be expressed as

$$Q_k = E\left[W_k W_k^T\right] = \sigma_{\mathrm{PAV}}^2 I_{2n\times 2n}. \tag{4}$$

In [2] and [3], σ_{PAV}^2 is selected as 0.05. $I_{2n\times 2n}$ is unit matrix.

C. OV Model

The OV model uses the measured signal and its orthogonal quantity as vectors to establish a state space [3], [21], [22]. The vectors are expressed as $X_k = [\,x_1\ x_2\ \cdots\ x_{2n-1}\ x_{2n}\,]^T$, where $x_1 = A_k\sin(\omega_k t_k + \theta_{1_k})$, $x_2 = A_k\cos(\omega_k t_k + \theta_{1_k})$, $x_{2n-1} = A_k\sin(n\omega_k t_k + \theta_{n_k})$, and $x_{2n} = A_k\cos(n\omega_k t_k + \theta_{n_k})$.

The measurement equation of OV model is expressed as

$$z_k = \begin{bmatrix} 1\ 0\ \cdots\ 1\ 0 \end{bmatrix} X_k + V_k. \tag{5}$$

The state equation of OV model is expressed as

$$X_{k+1} = \begin{bmatrix} \Phi_1 & \cdots & 0 \\ \vdots & \ldots & \vdots \\ 0 & \cdots & \Phi_n \end{bmatrix} X_k + W_k \tag{6}$$

where the state transition matrixes Φ_i are shown in the following:

$$\Phi_i = \begin{bmatrix} \cos(i\omega_k T) & \sin(i\omega_k T) \\ -\sin(i\omega_k T) & \cos(i\omega_k T) \end{bmatrix}. \tag{7}$$

The covariance matrix of state noise W_k for OV model can be expressed as

$$Q_k = E\left[W_k W_k^T\right] = \sigma_{\mathrm{OV}}^2 I_{2n\times 2n}. \tag{8}$$

In [3], [21], and [22], σ_{OV}^2 is selected as 0.05. $I_{2n\times 2n}$ is unit matrix.

III. DTM-KF ALGORITHM

In this section, the principle of DTM model is presented according to the theory of signal systems and stochastic process [51]–[53]. The covariance matrix of state noise for DTM model is defined according to the characteristics of ac signal. The state

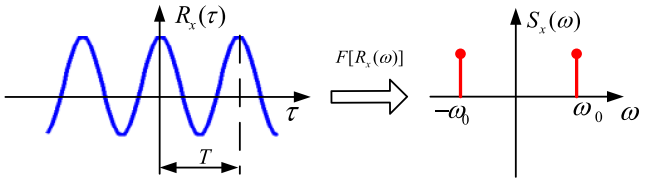

Fig. 1. Autocorrelation function and power spectral density of sinusoidal signal.

space dimension of DTM is expanded for the distorted ac signal, then DTM-KF algorithm is proposed.

A. Principle of DTM Model

The autocorrelation function and power spectral density of the pure sinusoidal signal $x(t) = A_m \sin(\omega_0 t + \theta)$ are shown in Fig. 1.

The correlation function of the pure sinusoidal signal can be expressed as

$$R_x(\tau) = \frac{A_m^2}{T}\int_0^T \sin(\omega_0 t)\sin(\omega_0 t+\tau)dt = \frac{A_m^2}{2}\cos(\omega_0\tau). \tag{9}$$

The power spectral density of the pure sinusoidal signal can be expressed as

$$\begin{aligned} S_x &= \int_{-\infty}^{+\infty} R_x(\tau)\cos\omega\tau d\tau = \frac{A_m^2}{2}\int_{-\infty}^{+\infty}\cos\omega_0\tau\cos\omega\tau d\tau \\ &= \frac{\pi A_m^2}{2}[\delta(\omega+\omega_0)+\delta(\omega-\omega_0)]. \end{aligned} \tag{10}$$

Since the power spectral density (10) contains an impulse function $\delta(\omega+\omega_0)$, the shaping filter cannot be directly determined [51]–[53]. The following function is considered:

$$H(\omega) = \pi\left[\delta(\omega+\omega_0)+\delta(\omega-\omega_0)\right]. \tag{11}$$

The white noise $w(t)$ with a variance of $\frac{A_m^2}{2\pi}$ is output through $H(\omega)$. Equation (12) can be obtained as follows:

$$C(\omega) = \frac{A_m^2}{2\pi}\left\{\pi^2[\delta^2(\omega+\omega_0)+\delta^2(\omega-\omega_0)]\right\} \tag{12}$$

where $\delta(\omega+\omega_0)$ is an impulse function and $\delta^2(\omega+\omega_0) \approx \delta(\omega+\omega_0)$. When comparing (10) and (12), their spectral characteristics and structure are very close. Equation (12) can be written as the following, when $H(\omega)$ is considered as a shaping filter:

$$\begin{aligned} S_x &= W(\omega)H(\omega)H^*(\omega) \\ &= \frac{A_m^2}{2\pi}\left\{\pi^2[\delta^2(\omega+\omega_0)+\delta^2(\omega-\omega_0)]\right\}. \end{aligned} \tag{13}$$

Since the second derivative of a pure sinusoidal signal can be expressed as

$$\ddot{x}(t) = -\omega_0^2 x(t) + w(t) \tag{14}$$

where $w(t)$ is the input white noise $w(t) \sim (0, \sigma_w^2)$, the variance of state noise σ_w^2 can be expressed as follows by contrasting (12):

$$\sigma_w^2 = \frac{A_m^2}{2\pi}. \tag{15}$$

Let $X(t) = [x(t)\ \dot{x}(t)]^T$ and the following equation can be obtained according to (14):

$$\begin{aligned} \frac{dX(t)}{dt} &= \begin{bmatrix}\dot{x}(t)\\ \ddot{x}(t)\end{bmatrix} = AX(t)+Bw(t) \\ &= \begin{bmatrix}0 & 1\\ -\omega_0^2 & 0\end{bmatrix}\begin{bmatrix}x(t)\\ \dot{x}(t)\end{bmatrix} + \begin{bmatrix}0\\1\end{bmatrix}w(t). \end{aligned} \tag{16}$$

Equation (16) is discretized, and the state equation can be obtained as follows:

$$\begin{aligned} X_{k+1} &= \begin{bmatrix}x\\ \dot{x}\end{bmatrix}_{k+1} = \Phi_k X_k + W_k \\ &= \begin{bmatrix}\cos(\omega_k T) & \sin(\omega_k T)/\omega_k \\ -\omega_k\sin(\omega_k T) & \cos(\omega_k T)\end{bmatrix}\begin{bmatrix}x\\ \dot{x}\end{bmatrix}_k \\ &\quad + \int_{kT}^{(k+1)T}\begin{bmatrix}\frac{1}{\omega_0}\sin(\omega_0 T)\\ \cos(\omega_0 T)\end{bmatrix}w(\tau)d\tau. \end{aligned} \tag{17}$$

The covariance matrix of state noise W_k can be expressed as

$$\begin{aligned} Q_k &= E\left[W_k W_k^T\right] \\ &= \sigma_w^2\begin{bmatrix}\frac{2\omega_k T-\sin(2\omega_k T)}{4\omega_k^3} & \frac{\sin^2(\omega_k T)}{2\omega_k^2} \\ \frac{\sin^2(\omega_k T)}{2\omega_k^2} & \frac{T}{2}+\frac{\sin(2\omega_k T)}{4\omega_k}\end{bmatrix}. \end{aligned} \tag{18}$$

Equations (15), (17), and (18) are the discretization DTM model. The discretization process of the DTM model can be referred to Appendix A.

B. Dimension Expansion of DTM Model

The state space dimension of the distorted ac signal is extended under the consideration of fundamental and low-order harmonic components. The vector is expressed as $X(t) = [x_1(t)\ \dot{x}_1(t)\ x_2(t)\ \dot{x}_2(t)\ \cdots\ x_n(t)\ \dot{x}_n(t)]^T$, where $\dot{x}_i(t)$ is the first derivative of $x_i(t)$. The state space expression of continuous time is established as follows:

$$\frac{dX(t)}{dt} = \begin{bmatrix}M_1 & 0 & \cdots & 0\\ 0 & M_2 & 0 & \vdots\\ \vdots & 0 & \ddots & 0\\ 0 & \cdots & 0 & M_n\end{bmatrix}X(t) + \begin{bmatrix}w_1(t)\\ w_2(t)\\ \vdots\\ w_n(t)\end{bmatrix} \tag{19}$$

where $[w_1(t)\ w_2(t)\ \cdots\ w_n(t)]^T$ is the state noise vector and $M_1 = \left[\begin{smallmatrix}0 & 1\\ -\omega_0^2 & 0\end{smallmatrix}\right]$, $M_2 = \left[\begin{smallmatrix}0 & 1\\ -(3\times\omega_0)^2 & 0\end{smallmatrix}\right]$, and $M_n = \left[\begin{smallmatrix}0 & 1\\ -(i\omega_0)^2 & 0\end{smallmatrix}\right]$.

The measurement equation can be expressed as

$$z(t) = \begin{bmatrix}1 & 0 & 1 & 0 & \cdots & 1 & 0\end{bmatrix}X(t) + v(t) \tag{20}$$

where $v(t)$ is the measurement noise vector.

Equations (19) and (20) are discretized according to the principle of DTM model. Then,

$$X_{k+1} = \Phi_k X_k + W_k = \begin{bmatrix} \Phi_1 & 0 & \cdots & 0 \\ 0 & \Phi_2 & \cdots & 0 \\ \vdots & \vdots & \ddots & \vdots \\ 0 & 0 & \cdots & \Phi_n \end{bmatrix}_k X_k + \begin{bmatrix} W_1 \\ W_2 \\ \vdots \\ W_n \end{bmatrix}_k \tag{21}$$

where $X_k = [\, x_{1k}\ \dot{x}_{1k}\ x_{2k}\ \dot{x}_{2k}\ \cdots\ \dot{x}_{nk}\ \dot{x}_{nk}\,]^T$ and Φ_k is the state transition matrix. $[\, W_1\ W_2\ \cdots\ W_n\,]_k^T$ is the state noise.

$$z_k = H_k X_k + V_k = \begin{bmatrix} 1\ 1\ 0\ 1\ 0 \cdots\ 1\ 0 \end{bmatrix} X_k + V_k \tag{22}$$

where H_k is the measurement transfer matrix and V_k is the measurement noise. The covariance of V_k can be expressed as $R_k = E[V_k V_k^T]$.

The state transition matrices of the fundamental and harmonic components can be expressed as

$$\Phi_{1_k} = \begin{bmatrix} \cos(\omega_k T) & \dfrac{\sin(\omega_k T)}{\omega_k} \\ -\omega_k \sin(\omega_k T) & \cos(\omega_k T) \end{bmatrix} \tag{23}$$

$$\Phi_{n_k} = \begin{bmatrix} \cos(i\omega_k T) & \dfrac{\sin(i\omega_k T)}{i\omega_k} \\ -i\omega_k \sin(i\omega_k T) & \cos(i\omega_k T) \end{bmatrix}. \tag{24}$$

The covariance matrices of state noise can be obtained as follows:

$$Q_{1_k} = \sigma_{w_1}^2 \begin{bmatrix} \dfrac{2\omega_k T - \sin(2\omega_k T)}{4\omega_k^3} & \dfrac{\sin^2(\omega_k T)}{2\omega_k^2} \\ \dfrac{\sin^2(\omega_k T)}{2\omega_k^2} & \dfrac{T}{2} + \dfrac{\sin(2\omega_k T)}{4\omega_k} \end{bmatrix} \tag{25}$$

$$Q_{i_k} = \sigma_{w_i}^2 \begin{bmatrix} \dfrac{2i\omega_k T - \sin(2i\omega_k T)}{4i^3\omega_k^3} & \dfrac{\sin^2(i\omega_k T)}{2i^2\omega_k^2} \\ \dfrac{\sin^2(i\omega_k T)}{2i^2\omega_k^2} & \dfrac{T}{2} + \dfrac{\sin(2i\omega_k T)}{4i\omega_k} \end{bmatrix}. \tag{26}$$

Equations (19) and (20) are the discretization DTM models. By comparing state space expression of the DTM model (19) with that of the OV model (6), it can be found that the state transition expressions of these two tracking models are the same regardless of the state noise. However, the difference between the two models is that the DTM model can obtain the state noise covariance matrix by (15), (25), and (26). The covariance matrices of state noise for the PAV and OV models are all unit matrices in (4) and (8). The DTM model clearly shows the interrelationship of the state noise between the estimated vectors. So, it is theoretically superior to the PAV and OV model [51].

C. DTM-KF Algorithm

The linear discrete DTM-KF algorithm can be expressed as follows by combining DTM model [51]:

$$\begin{cases} \hat{X}_{k+1/k} = \Phi_k \hat{X}_{k/k} \\ P_{k+1/k} = \Phi_k P_{k/k} \Phi_k^T + Q_k \\ K_{k+1} = P_{k+1/k} H_k^T \left(H_k P_{k+1/k} H_k^T + R_k \right)^{-1} \\ \hat{X}_{k+1/k+1} = \hat{X}_{k+1/k} + K_{k+1} \left(Z_{k+1} - H_k \hat{X}_{k+1/k} \right) \\ P_{k+1/k+1} = P_{k+1/k} - K_{k+1} H_k P_{k+1/k}. \end{cases} \tag{27}$$

In the second step of (27) $P_{k+1/k} = \Phi_k P_{k/k} \Phi_k^T + Q_k$, where $P_{k/k} = E[\tilde{X}_{k/k} \tilde{X}_{k/k}^T]$ and $\tilde{X}_{k/k}$ is the error between the true value X_k and the estimated value $\hat{X}_{k/k}$, that is $\tilde{X}_{k/k} = X_k - \hat{X}_{k/k}$. The role of $Q_k = E[w_k w_k^T]$ is to compensate for the precision of $P_{k/k}$, which ultimately determines the accuracy of $P_{k+1/k}$. If Q_k is only the unit matrix, then the cross-correlated elements of $\hat{X}_{k/k}$ cannot be effectively compensated. It causes a loss of precision. Therefore, the importance of Q_k derived in this paper is theoretically verified.

From state estimation value of the first derivative $\hat{\dot{x}}_{i_{k+1}}$ for the fundamental and harmonic components, the orthogonal estimation value $\hat{y}_{i_{k+1}}\,(\omega_k \neq 0)$ of $\hat{x}_{i_{k+1}}$ is obtained.

$$\hat{y}_{i_{k+1}} = \left(\frac{\hat{\dot{x}}_{i_{k+1}}}{\omega_k} \right). \tag{28}$$

Further, the amplitude and the phase angle for the fundamental and harmonic components can be calculated as follows:

$$A_{i_{k+1}} = \sqrt{\hat{x}_{i_{k+1}}^2 + \hat{y}_{i_{k+1}}^2} \tag{29}$$

$$\phi_{i_{k+1}} = \arctan\left(\frac{\hat{x}_{i_{k+1}}}{\hat{y}_{i_{k+1}}} \right). \tag{30}$$

When the KF algorithm is tracking, it mainly involves the selection of the measurement noise R and covariance matrices of state noise Q_{i_k}. R can be selected according to the sensor error. The typical sensor error is $\pm 1\%$ of the range. Q_{i_k} can be obtained according to (26). Taking the ac voltage as an example, the maximum amplitude of the voltage is selected as A_{m_1} in the fundamental component Q_{1_k}, and the low-order harmonic contents are 20–40% of the fundamental component, that is, $A_{m_i} = (0.2\text{–}0.4) \times A_{m_1}$ in Q_{i_k}. Furthermore, the filter coefficient λ of $Q = \lambda \times Q_{i_k}$ is selected according to requirement of the project tracking. If high dynamic response speed is demanded, $\lambda = 0.1\text{–}1$. If high tracking accuracy is demanded, $\lambda < 0.1$. In this paper, λ is selected as 0.05.

IV. Simulation and Evaluation

In this section, three algorithms of proposed DTM-KF, OV-KF, and PAV-KF are evaluated and compared by simulation. The root mean squared error (RMSE) values are used as statistical indicators for evaluation. The harmonics ratio for voltage (HRU) is used as a statistical indicator for harmonics evaluation. First of all, the formula of digital simulation and the state noise variance

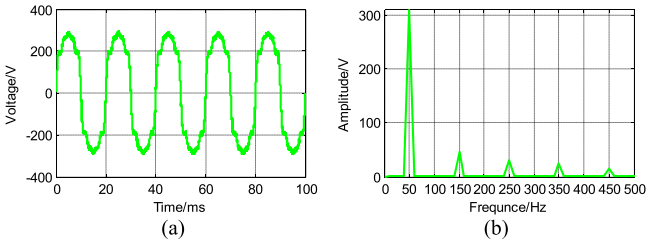

Fig. 2. Simulation data and spectrogram. (a) Simulation data. (b) Spectrogram of simulation data.

selection of algorithms are given. Then, the tracking comparison results of fundamental and harmonics component are evaluated and compared by RMSE and HRU values.

A. Simulation Settings

The formula of digital simulation for distorted ac voltage signal with harmonics components is as follows:

$$\mathrm{u}(t) = 220\sqrt{2} \times [1.0\sin(\omega t) + 0.15\sin(3\omega t) + 0.1\sin(5\omega t) + 0.08\sin(7\omega t) + 0.05\sin(9\omega t)] + 3.11v(t)\,. \tag{31}$$

The amplitude of the fundamental component is $220\sqrt{2}$V. The harmonic components are set as percentages of fundamental component: 15% of 3rd, 10% of 5th, 8% of 7th, and 5% of 9th. $\sigma_v = 3.11$V of the measurement white noise is superimposed, that is, $\sigma_v = 0.01 \times 220\sqrt{2} = 3.11$ V. $\omega = 2 \times \pi \times 50$, The sampling frequency is selected to be 2000×50 Hz. The simulation data are shown in Fig. 2(a). The spectrogram of simulation data is shown in Fig. 2(b).

R of three algorithms is selected as 3. 11 V. The covariance matrices of state noise are selected as follows:

1) *DTM-KF algorithm:* The covariance of the fundamental component is $Q_i = 0.05 \times Q_{ik}$. The amplitudes A_{m_i} of third harmonics are $A_{m_3} = 0.4 \times A_{m_1}$ V, owing to the content of third harmonics generally higher in distorted ac signal. The amplitudes A_{m_i} of other harmonics components are $A_{m_i} = 0.2 \times A_{m_1}$ V. The amplitude A_{m_1} of the fundamental component is $A_{m_1} = 220\sqrt{2}$ V.
2) *OVKF and PAV-KF algorithms:* The covariance of fundamental and harmonics components are all $Q_i = 0.05 \times I_{10\times 10}$. These parameters are the same as in the literature [2], [3], [21], [22].

The initial covariance matrices of three algorithms in (27) are selected as $P_{0/0} = 1000 \times I_{10\times 10}$.

B. Comparison Results of Fundamental Component

The tracking results of the fundamental component are shown in Fig. 3. The RMSE results of the fundamental component evaluated by 100 times Monte Carlo simulations are shown in Fig. 4(a). From Figs. 3 and 4(a), it can be seen that the tracking results of the three algorithms are smooth only after the first cycle. So, the RMSE results for 20–100 ms are evaluated and shown in Fig. 4(b) and Table II.

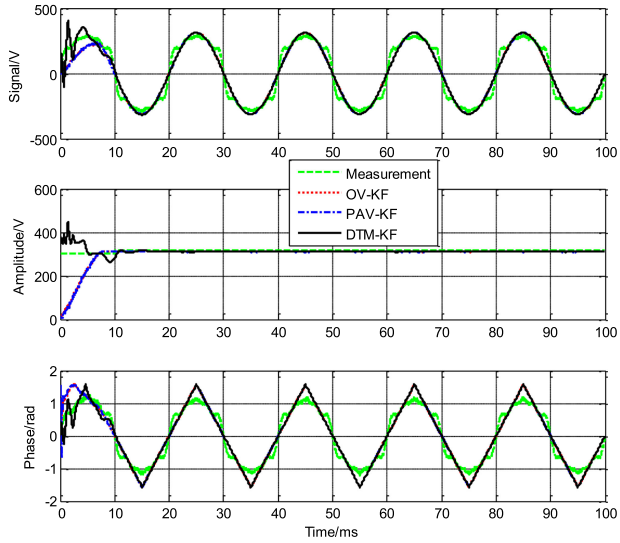

Fig. 3. Tracking results of the fundamental component.

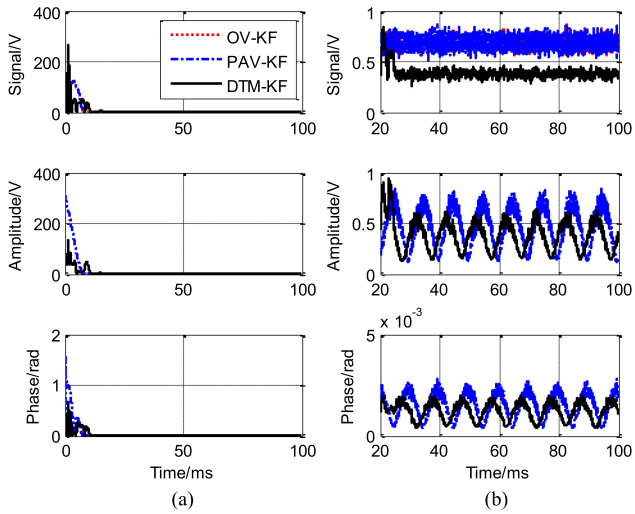

Fig. 4. RMSE results of the fundamental component. (a) RMSE results for all time. (b) RMSE results for 20–100 ms.

TABLE II
FUNDAMENTAL TRACKING COMPARISON RESULTS

Algorithms	RMSE for fundamental tracking (p.u.)		
	Signal	Amplitude	Phase
OV-KF	0.688109	0.467062	0.001496
PAV-KF	0.687722	0.467062	0.001496
DTM-KF	0.389317	0.383468	0.001222

RMSE is defined as follows:

$$\mathrm{RMSE} = \sqrt{\frac{1}{N}\sum_{k=1}^{N}\left(x_{ij} - \hat{x}_{ij}^{k}\right)^2} \tag{32}$$

where N is number of simulations, $N = 100$; x_{ij} and $\hat{x}_{ij}$ are j-sampled values of x_i and $\hat{x}_i$, respectively.

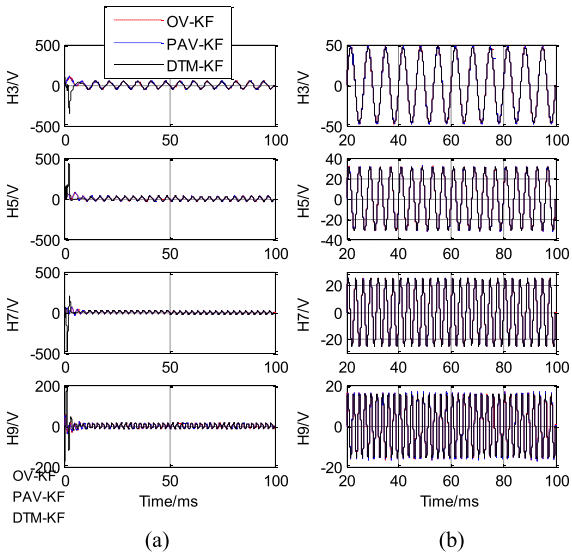

Fig. 5. Tracking comparison results of harmonics components. (a) Tracking results for all time. (b) Tracking results for 20–100 ms.

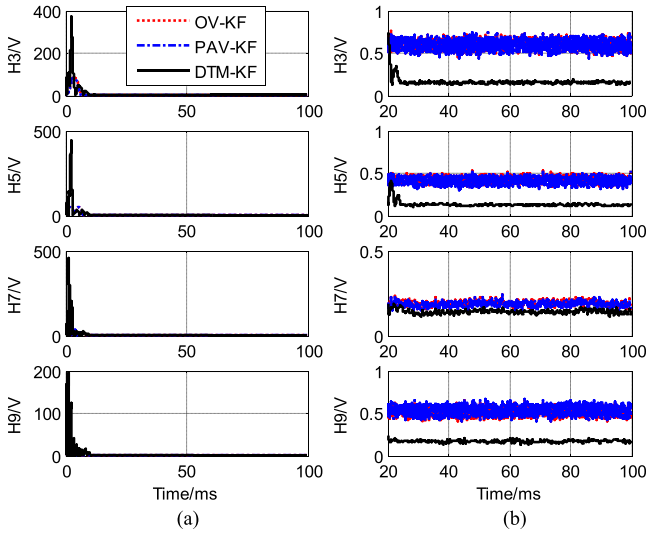

Fig. 6. RMSE comparison results of harmonics components. (a) RMSE results for all time. (b) RMSE results for 20–100 ms.

As shown in Fig. 4(b) and Table II, all three algorithms accurately track the values of signal, amplitude, and phase. The RMSE results of the DTM-KF are minimal. It proves that the proposed DTM-KF is accurate and effective for tracking the fundamental component.

C. Comparison Results of Harmonics Component

The tracking comparison results of harmonics components are shown in Fig. 5. The RMSE comparison results of harmonics components for all time are shown in Fig. 6(a). The third, fifth, seventh, and ninth harmonic components are expressed as H3, H5, H7, and H9, respectively. The RMSE comparison results for 20–100 ms are shown in Fig. 6(b) and Table III. As shown in Fig. 6(b) and Table III, it can be seen that the RMSE results of the DTM-KF are minimal. It verifies that the proposed DTM-KF is accurate and effective for the estimation of harmonics components.

TABLE III
RMSE COMPARISON RESULTS HARMONICS ESTIMATION

Algorithms	RMSE for harmonics estimation (V)			
	H3	H5	H7	H9
OV-KF	0.599435	0.418311	0.191220	0.519606
PAV-KF	0.596086	0.410001	0.187065	0.532739
DTM-KF	0.162753	0.132910	0.141346	0.168688

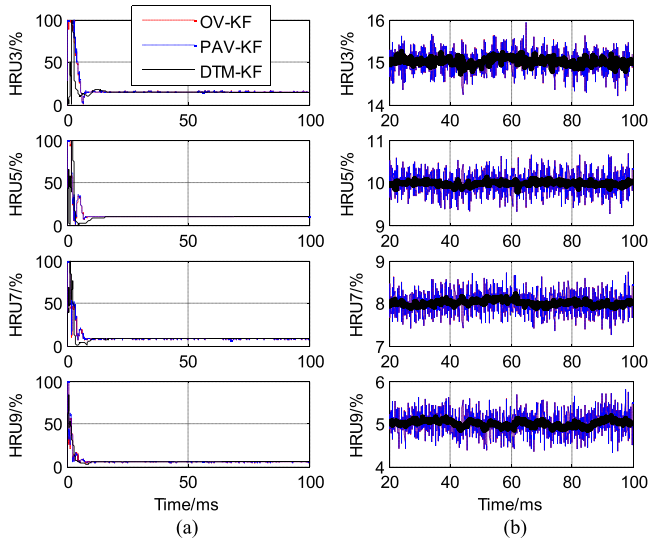

Fig. 7. HRU tracking comparison results of harmonics components. (a) HRU tracking results for all time. (b) HRU tracking results for 20–100 ms.

The HRU statistical evaluation are carried out for quantitatively instructing harmonics components. HRU is defined as follows:

$$\mathrm{HRU_n} = \frac{U_n}{U_1} \times 100\% \tag{33}$$

where U_1 is the voltage rms value of fundamental component and U_n is the voltage rms value of nth harmonic components.

The HRU tracking comparison results of harmonics components are shown in Fig. 7. From the HRU tracking results for 20–100 ms in Fig. 7(b), it can be obviously seen that estimation results of the DTM-KF are minimal. The comparison results of HRU RMSE for all time are shown in Fig. 8(a). The HRU RMSE comparison results for 20–100 ms are shown in Fig. 8(b) and Table IV.

From Fig. 8(b) and Table IV, it can be obviously seen that the accuracy of the DTM-KF algorithm is higher than that of the OV-KF and PAV-KF algorithms.

V. EXPERIMENTAL AND EVALUATION

In this paper, the sampling data of distorted ac signals through the experimental platform are used for the evaluation of

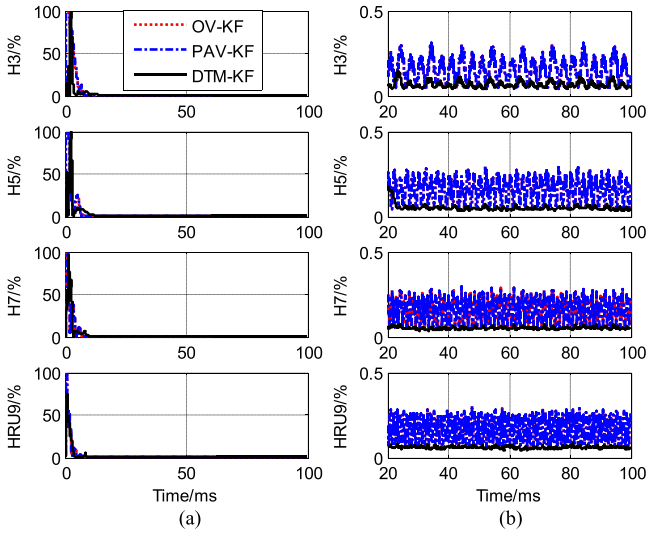

Fig. 8. HRU RMSE comparison results of harmonics components. (a) HRU RMSE results for all time. (b) HRU RMSE results for 20–100 ms.

TABLE IV
HRU RMSE COMPARISON RESULTS FOR HARMONICS

Algorithms	RMSE of harmonics HRU (%)			
	H3	H5	H7	H9
OV-KF	0.151379	0.153897	0.158027	0.167611
PAV-KF	0.151379	0.153896	0.158026	0.167611
DTM-KF	0.066050	0.050067	0.052350	0.059389

three algorithms. The tracking results of DTM-KF, OV-KF, and PAV-KF are compared, respectively. First, there is a brief introduction to the experimental settings. Second, the tracking comparison results of the fundamental component are obtained. Third, the tracking comparison results of harmonics components are presented.

A. Experimental Settings

The experimental platform and data sampling are shown in Fig. 9(a). The experimental platform includes devices such as programmable power supply, programmable line configuration, and programmable *RLC* load.

The experimental platform can simulate faults such as the grid power, transmission line, and load according to user's needs. The experiment of superimposing harmonics in fundamental voltage is carried out through programmable power supply device. The HRU of harmonic components are set as follows: 10% of third, 3% of fifth, and 10% of seventh. The principle diagram of the programmable power supply is shown as Fig. 9(b). The sampling data are shown in Fig. 9(c). The spectrogram of sampling data is shown in Fig. 9(d). In the experimental data sampling, the voltage signals are sampled by the oscilloscope of Tektronix GDS-2102. The sampling frequency is selected to be 2000 × 50 Hz.

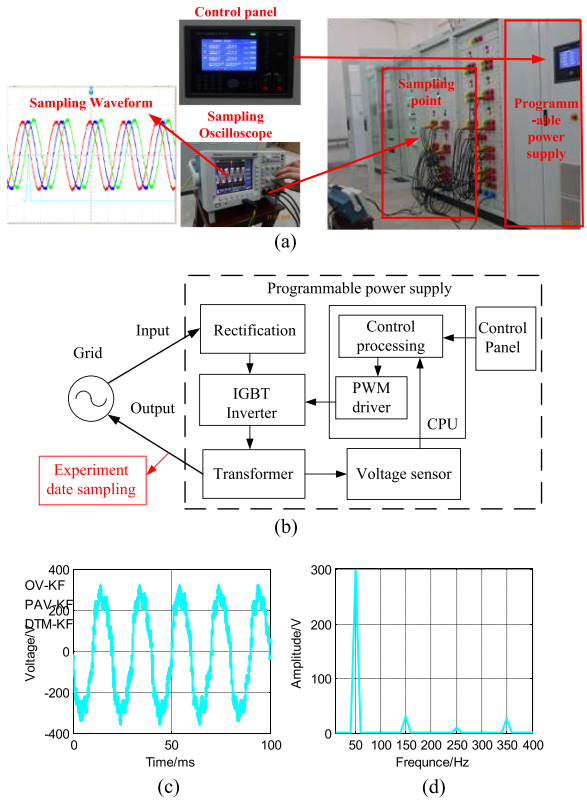

Fig. 9. Experiment platform and experiment data sampling. (a) Experiment platform and data sampling. (b) Principle diagram of the programmable power supply. (c) Sampling data. (d) Spectrogram of sampling data.

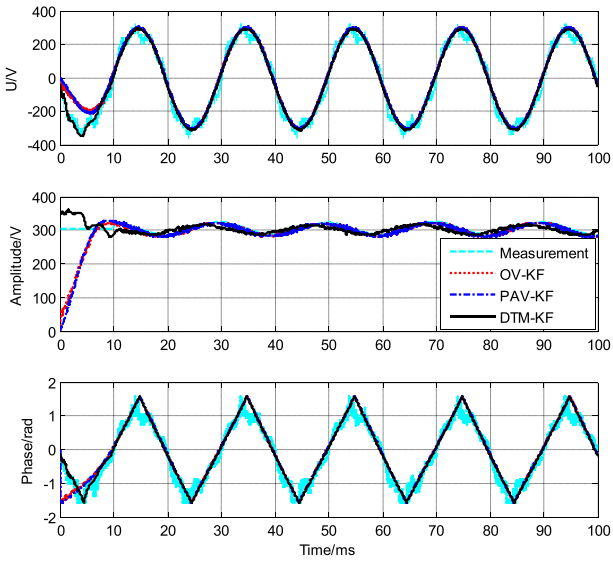

Fig. 10. Tracking comparison results of fundamental component.

B. Comparison Results of Fundamental Component

The model parameters of the three algorithms still adopt the values of the simulation evaluation in Section IV. The tracking comparison results of the signal, amplitude, and phase for the three algorithms are shown in Fig. 10. It can be seen from Fig. 10 that the tracking results of the three algorithms are smooth after

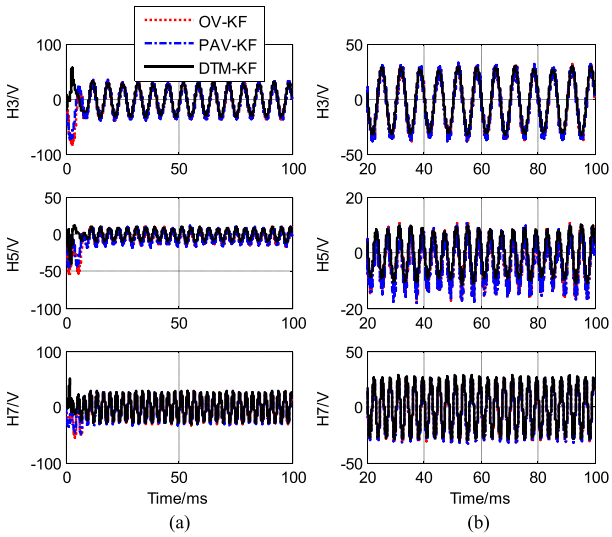

Fig. 11. Tracking comparison results of harmonics components. (a) Tracking results for all time. (b) Tracking results for 20–100 ms.

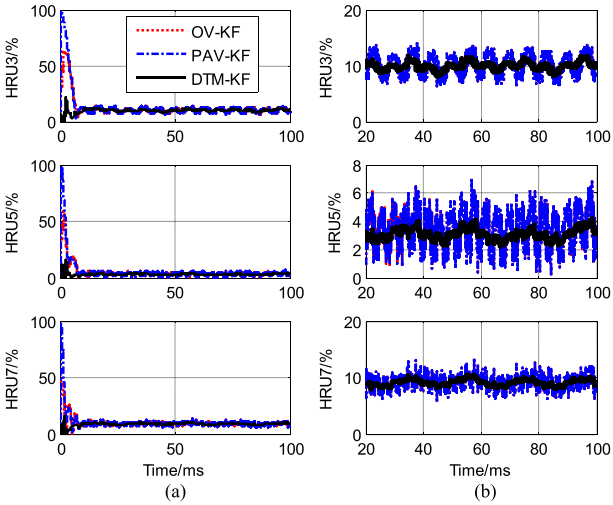

Fig. 12. HRU tracking comparison results of harmonics components. (a) HRU results for all time. (b) HRU results for 20–100 ms.

the first signal cycle. It is difficult to distinguish the advantages and disadvantages of three algorithms from the fundamental waveform tracking. So, the tracking comparisons of harmonics components are carried out.

C. Comparison Results of Harmonics Components

The tracking comparison results of harmonics components for all time are shown in Fig. 11(a). The tracking results for 20–100 ms are shown in Fig. 11(b). It can be seen from Fig. 11(b) that the tracking error of DTM-KF is small, especially the tracking error of the third and fifth harmonics components is obviously small.

The HRU tracking comparison results of harmonics components for all time are shown in Fig. 12(a). The HRU tracking results for 20–100 ms are shown in Fig. 12(b).

It can be seen from Fig. 12(b) that the tracking results of the DTM-KF algorithm are closest to the HRU values of harmonic components for experimental setting. That is, the DTM-KF algorithm tracking error is the smallest and obviously superior to the OV-KF and PAV-KF algorithms. It shows that the proposed DTM-KF algorithm is effective and has the highest tracking accuracy.

VI. Conclusion

This paper presented a new DTM-based linear KF (DTM-KF) algorithm for the real-time detection of grid voltage fundamental and harmonic components. The DTM model had a clear physical meaning for the covariance matrix of state noise. It clearly depicted the interrelationship between the estimated vectors for distorted ac signal. The following conclusion could be drawn through a lot of simulations and experiments: For both the fundamental and harmonic components, the tracking accuracy of the proposed DTM-KF algorithm is higher than the traditional models–based KF algorithms.

Appendix

A. Discretization of DTM Model

The two order derivative of $x(t) = \sin(\omega_0 t + \theta)$ can be expressed as

$$\ddot{x}(t) = -\omega_0^2 x(t) + w(t) \tag{A1}$$

where $w(t)$ is white noise with a mean value of 0 and a variance of σ_ω^2.

Equation (A2) can be obtained for $X(t) = [\,x(t)\ \dot{x}(t)\,]^T$ as follows:

$$\dot{X}(t) = AX(t) + Bw(t) \tag{A2}$$

where $A = \left[\begin{smallmatrix} 0 & 1 \\ -\omega_0^2 & 0 \end{smallmatrix}\right]$ and $B = \left[\begin{smallmatrix} 0 \\ 1 \end{smallmatrix}\right]$.

Equation (A2) is integrated for the time interval T. Equation (A3) can be obtained as

$$X(t+T) = e^{AT}X(t) + \int_t^{t+T} e^{A(t+T-\tau)}Bw(\tau)d\tau \tag{A3}$$

where

$$\begin{cases} \Phi_k = e^{AT} \\ W_k = \int_{kT}^{(k+1)T} e^{A[(k+1)T-\tau]}Bw(\tau)d\tau \end{cases}. \tag{A4}$$

The state transition matrix Φ_k can be expressed as

$$\begin{aligned} \Phi_k = e^{AT} &= L^{-1}([sI - A]^{-1}) \\ &= \begin{bmatrix} \cos(\omega_0 T) & \dfrac{1}{\omega_0}\sin(\omega_0 T) \\ -\omega_0 \sin(\omega_0 T) & \cos(\omega_0 T) \end{bmatrix}. \end{aligned} \tag{A5}$$

The state noise W_k satisfies (A6) as follows:

$$W_k = \int_{kT}^{(k+1)T} e^{A[(k+1)T-\tau]} \begin{bmatrix} 0 \\ 1 \end{bmatrix} w(\tau) d\tau = \int_{kT}^{(k+1)T} \begin{bmatrix} \frac{1}{\omega_0}\sin(\omega_0 T) \\ \cos(\omega_0 T) \end{bmatrix} w(\tau) d\tau. \quad \text{(A6)}$$

The covariance matrix of the state noise W_k can be expressed as

$$Q(k) = E\left[W_k W_k^T\right] = \sigma_\omega^2 \begin{bmatrix} \frac{2\omega_0 T - \sin(2\omega_0 T)}{4\omega_0^3} & \frac{\sin^2(\omega_0 T)}{2\omega_0^2} \\ \frac{\sin^2(\omega_0 T)}{2\omega_0^2} & \frac{T}{2} + \frac{\sin(2\omega_0 T)}{4\omega_0} \end{bmatrix}. \quad \text{(A7)}$$

ACKNOWLEDGMENT

The author would like to thank Haoyao Nie for her help in this paper.

REFERENCES

[1] F. Auger *et al.*, "Industrial applications of the Kalman filter: A review," *IEEE Trans. Ind. Electron.*, vol. 60, no. 12, pp. 5458–5471, Dec. 2013.

[2] A. A. Girgis and R. G. Brown, "Application of Kalman filtering in computer relaying," *IEEE Trans. Power App. Syst.*, vol. PAS-100, no. 7. pp. 3387–3397. Jul. 1981.

[3] A. A. Girgis, W. B. Chang, and E. B. Makram, "A digital recursive measurement scheme for online tracking of power system harmonics," *IEEE Trans. Power Del.*, vol. 6, no. 3, pp. 1153–1160, Jul. 1991.

[4] J. Enayati and Z. Moravej, "Real-time harmonic estimation using a novel hybrid technique for embedded system implementation," *Int. Trans. Elect. Energ. Syst.*, vol. 2, no. 12, Oct. 2017, pp. 1–13, doi: 10.1002/etep.2428.

[5] J. Enayati and Z. Moravej, "Real-time harmonics estimation in power systems using a novel hybrid algorithm," *IET Gener. Transmiss. Distribution*, vol. 14, no. 11. pp. 3532–3538, Oct. 2017.

[6] R. C. Magaña, A. Medina, and O. A. Lara, "Time-domain harmonic state estimation of nonlinear load power systems with under-determined condition based on the extended Kalman filter," *Int. Trans. Electr. Energ. Syst.*, vol. 27, no. 2, Jul. 2017, pp. 1–22, doi: 10.1002/etep.2242.

[7] R. Panigrahi and B. Subudhi, "Performance enhancement of shunt active power filter using a Kalman filter-based H$^\infty$ control strategy," *IEEE Trans. Power Electron.*, vol. 32, no. 4, pp. 2622–2630, Apr. 2017.

[8] J. R. Maldonado, "Total harmonic distortion estimation, minimization inter harmonic amplitude and expanding bands rejection in TKF filters," *IEEE Latin Amer. Trans.*, vol. 14, no. 2, pp. 652–656, Feb. 2016.

[9] H. Hajimolahoseini, R. Amirfattahi, and H. S. Zadeh, "Instantaneous fundamental frequency estimation of nonstationary periodic signals using nonlinear recursive filters," *IET Signal Process.*, vol. 9, no. 2, pp. 143–153, Apr. 2015.

[10] P. K. Ray and B. Subudhi, "Ensemble-Kalman-filter-based power system harmonic estimation," *IEEE Trans. Instrum. Meas.*, vol. 61, no. 12, pp. 3216–3224, Dec. 2012.

[11] K. H. Kwan, P. L. So, and Y. C. Chu, "An output regulation-based unified power quality conditioner with Kalman filters," *IEEE Trans. Ind. Electron.*, vol. 59, no. 11, pp. 4248–4262, Nov. 2012.

[12] S. H. Jo *et al.*, "Kalman-filter-based multilevel analysis to estimate electric load composition," *IEEE Trans. Ind. Electron.*, vol. 59, no. 11, pp. 4263–4271, Nov. 2012.

[13] A. Medina and R. C. Magana, "Time-domain harmonic state estimation based on the Kalman filter poincare map and extrapolation to the limit cycle," *IET Gener. Transmiss. Distribution*, vol. 6, no. 12, pp. 1209–1217, Dec. 2012.

[14] J. Antonio, O. Serna, and J. R. Maldonado, "Taylor–Kalman–Fourier filters for instantaneous oscillating phasor and harmonic estimates," *IEEE Trans. Instrum. Meas.*, vol. 61, no. 4, pp. 941–951, Apr. 2012.

[15] S. K. Singh, N. Sinha, and A. K. Goswami, "Several variants of Kalman filter algorithm for power system harmonic estimation," *Int. J. Elect. Power Energy Syst.*, vol. 78, pp. 793–800, Jan. 2016.

[16] P. K. Ray, P. S. Puhan, and G. Panda, "Real time harmonics estimation of distorted power system signal," *Int. J. Elect. Power Energy Syst.*, vol. 75, pp. 91–98, Sep. 2016.

[17] D. H. Dini and D. P. Mandic, "Widely linear modeling for frequency estimation in unbalanced three-phase power systems," *IEEE Trans. Instrum. Meas.*, vol. 62, no. 2, pp. 353–363, Feb. 2013.

[18] S. Reza, M. Ciobotaru, and V. G. Agelidi, "Accurate estimation of single-phase grid voltage fundamental amplitude and frequency by using a frequency adaptive linear kalman filter," *IEEE J. Emerg. Sel. Topics Power Electron.*, vol. 4, no. 4, pp. 1226–1235, Dec. 2016.

[19] H. K. Sahoo, P. K. Dash, and N. P. Rath, "Frequency estimation of distorted nonstationary signals using complex H∞ filter," *Int. J. Electron. Commun.*, vol. 66, pp. 267–274, Aug. 2012.

[20] H. Hajimolahoseini, M. R. Taban, and H. S. Zadeh, "Extended Kalman filter frequency tracker for nonstationary harmonic signals," *Measurement*, vol. 45, pp. 126–132, Sep. 2012.

[21] R. Cardoso, R. F. Camargo, H. Pinheiro, and H. A. Grundling, "Kalman filter based synchronisation methods," *IET Gener. Transmiss. Distribution*, vol. 2, no. 4, pp. 542–555, Jun. 2008.

[22] A. Bagheri, M. Mardaneh, A. Rajaei, and A. Rahideh, "Detection of grid voltage fundamental and harmonic components using Kalman filter and generalized averaging method," *IEEE Trans. Power Electron.*, vol. 31, no. 2, pp. 1064–1073, Feb. 2016.

[23] J. M. Kanieski, R. Cardoso, and H. Pinheiro, "Kalman filter-based control system for power quality conditioning devices," *IEEE Trans. Ind. Electron.*, vol. 60, no. 11, pp. 5214–5227, Nov. 2013.

[24] J. M. Kanieski, R. V. Tambara, H. Pinheiro, R. Cardoso, and H. A. Gründling, "Robust adaptive controller combined with a linear quadratic regulator based on Kalman filtering," *IEEE Trans. Autom. Control*, vol. 61, no. 5, pp. 1373–1378, May 2016.

[25] X. Wang and E. E. Yaz, "Smart power grid synchronization with fault tolerant nonlinear estimation," *IEEE Trans. Power Syst.*, vol. 31, no. 6, pp. 4806–4816, Nov. 2016.

[26] M. Chakir, I. Kamwa, and H. L. Huy, "Extended C37. 118. 1 PMU algorithms for joint tracking of fundamental and harmonic phasors in stressed power systems and microgrids," *IEEE Trans. Power Del.*, vol. 29, no. 3, pp. 1465–1480, Jun. 2014.

[27] D. Dotta and J. H. Chow, "Second harmonic filtering in phasor measurement estimation," *IEEE Trans. Power Del.*, vol. 28, no. 2, pp. 1240–1241, Apr. 2013.

[28] C. Huang, X. Xie, and H. Jiang, "Dynamic phasor estimation through DSTKF under transient conditions," *IEEE Trans. Instrum. Meas.*, vol. 66, no. 11, pp. 2929–2936, Nov. 2017.

[29] A. Abdolkhalig and R. Zivanovic, "Phasor measurement based on IEC 618 50-9-2 and Kalman-filtering,"*Measurement*, vol. 50, pp. 126–134, *Jan.* 2014.

[30] I. Kamwa, S. R. Samantaray, and G. Joos, "Wide frequency range adaptive phasor and frequency PMU algorithms," *IEEE Trans. Smart Grid*, vol. 5, no. 2, pp. 569–679, Mar. 2014.

[31] I. Kamwa, S. R. Samantaray, and G. Joos, "Compliance analysis of PMU algorithms and devices for wide-area stabilizing control of large power systems," *IEEE Trans. Power Syst.*, vol. 28, no. 2, pp. 1766–1778, May 2013.

[32] N. Kose, O. Salor, and K. Leblebicioglu, "Kalman filtering based approach for light flicker evaluation of power systems," *IET Gener. Transmiss. Distribution*, vol. 5, no. 1, pp. 57–69, Jan. 2011.

[33] I. Sadinezhad and V. G. Agelidis, "Frequency adaptive least-squares-Kalman technique for real-time voltage envelope and flicker estimation," *IEEE Trans. Ind. Electron.*, vol. 59, no. 8, pp. 3330–3341, Aug. 2012.

[34] H. Samet *et al.*, "Improvement of reactive power calculation in electric arc furnaces utilising kalman filter," *IET Sci. Meas. Technol.*, vol. 11, no. 3, pp. 241–248, May 2017.

[35] H. M. Al-Hamadi, "Fuzzy logic voltage flicker estimation using Kalman filter," *IEEE Trans. Elect. Power Energy Syst.*, vol. 36, no. 1, pp. 60–67, Mar. 2012.

[36] A. A. Abdelsalam, A. A. Eldesouky, and A. A. Sallam, "Classification of power system disturbances using linear Kalman filter and fuzzy-expert system," *Elect. Power Energy Syst.*, vol. 43, pp. 688–695, Jul. 2012.
[37] A. A. Abdelsalam, A. A. Eldesouky, and A. A. Sallam, "Characterization of power quality disturbances using hybrid technique of linear kalman filter and fuzzy-expert system," *Elect. Power Syst. Res.*, vol. 83, no. 1, pp. 41–50, Oct. 2012.
[38] H. K. Sahoo, and P. K. Dash, "Robust estimation of power quality disturbances using unscented H^{∞} filter," *Int. J. Elect. Power Energy Syst.*, vol. 73, pp. 438–447, May 2015.
[39] S. Zhao, B. Huang, and F. Liu, "Linear optimal unbiased filter for time-variant systems without apriori information on initial conditions," *IEEE Trans. Autom. Control*, vol. 62, no. 2, pp. 882–887, Feb. 2017.
[40] R. Panigrahi, B. Subudhi, and P. C. Panda, "A robust LQG servo control strategy of shunt-active power filter for power quality enhancement," *IEEE Trans. Power Electron.*, vol. 31, no. 4, pp. 2860–2869, Apr. 2016.
[41] R. Panigrahi, B. Subudhi, and P. C. Panda, "Model predictive-based shunt active power filter with a new reference current estimation strategy," *IET Power Electron.*, vol. 8, no. 2, pp. 221–233, Feb. 2015.
[42] A. Abdolkhalig and R. Zivanovic, "Simulation and testing of the over-current protection system based on IEC 61850 State-Buses and dynamic estimator," *Sustain. Energy, Grids Networks*, vol. 2, pp. 41–50, Apr. 2015.
[43] L. Helena, B. Liboni, M. C. Oliveira, and I. N. Silva, "On the problem of optimal estimation of balanced and symmetric three-phase signals," *Int. J.Elect. Power Energy Syst.*, vol. 91, pp. 155–165, Mar. 2017.
[44] J. M. Kanieski *et al.*, "Kalman filter-based control system for power quality conditioning devices," *IEEE Trans. Ind. Electron.*, vol. 60, no. 11, pp. 5214–5227, Nov. 2013.
[45] S. F. He, K. C. Li, and M. Zhang, "A new transient power quality disturbances detection using strong trace filter," *IEEE Trans. Instrum. Meas.*, vol. 63, no. 12, pp. 2863–2871, Dec. 2014.
[46] A. Moschitta, P. Carbone, and C. Muscas, "Performance comparison of advanced techniques for voltage dip detection," *IEEE Trans. Instrum. Meas.*, vol. 61, no. 5, pp. 1494–1502, May 2012.
[47] K. Sadigh and K. M. Smedley, "Fast and precise voltage sag detection method for dynamic voltage restorer (DVR) application," *Elect. Power Syst. Res.*, vol. 130, pp. 192–207, Sep. 2016.
[48] S. Arias, A. J. Ustariz, and E. A. Cano, "Detection of power quality disturbances using deformation tensor parameters," *IEEE Latin Amer. Trans.*, vol. 13, no. 7, pp. 2106–2113, Jul. 2015.
[49] D. Velasco a *et al.*, "Review of antiislanding techniques in distributed generators," *Renewable Sustain. Energy Rev.*, vol. 14, no. 6, pp. 1608–1614, Aug. 2010.
[50] A. R. D. Fazio *et al.*, "A smart device for islanding detection in distribution system operation," *Elect. Power Syst. Res.*, vol. 120, pp. 87–95, Aug. 2015.
[51] R. G. Brown and PYC Hwang, *Introduction to Random Signals and Applied Kalman Filtering with MATLAB Exercises*. 4th ed., Hoboken, NJ, USA: Wiley, 2011.
[52] A. V. Oppenheim, A. S. Willsky, and S. H. Nawab, *Signals and Systems*. 2nd ed., New Delhi: Prentice-Hall, 1997.
[53] S. Haykin and B. V. Veen, *Signals and Systems*. 2nd ed., Hoboken, NJ, USA: Wiley, 2003.

Xiaohua Nie (M'17) was born in 1969. He received the Ph.D. degree in electronic and electrical engineering from the China University of Mining and Technology, Xuzhou, China, in 2003.

He is currently an Associate Professor with the Department of Energy and Electrical Engineering, Nanchang University, Nanchang, China. As the Project Leader, his research has been supported by two of the National Natural Science Foundations of China. Their titles separately are "Research on MPPT control and quantitative evaluation methods for photovoltaic array under complex application condition" and "Research on Power Quality Dynamic Tracking and Real-time Detection Method for Microgrid Complex Source Load Environment." He has authored or coauthored various peer-reviewed journals. His research interests include state estimation and optimal control techniques with application to power system, power electronics, etc.